PCCP

Accepted Manuscript

ROYAL SOCIETY OF CHEMISTRY

www.rsc.org/pccp

Journal Name

RSCPublishing

COMMUNICATION

Hybrid inorganic-organic tandem solar cells for broad absorption of the solar spectrum

Cite this: DOI: 10.1039/x0xx00000x

M. J. Speirs[a], B. G. H. M. Groeneveld[a], L. Protesescu[b,c], C. Piliego[a], M. V. Kovalenko[b,c] and M. A. Loi[a]

Received 00th January 2012,
Accepted 00th January 2012

DOI: 10.1039/x0xx00000x

www.rsc.org/

We report the first hybrid tandem solar cell with solution processable active layers using colloidal PbS quantum dots (QDs) as the front subcell in combination with a polymer-fullerene rear subcell. Al/WO_3 is introduced as an interlayer, yielding an open circuit voltage (V_{OC}) equal to about 92 % of the sum of the V_{OC} of the subcells. The device exhibits a power conversion efficiency of 1.8 %. Optical simulations of various tandem configurations show that combining PbS QDs with small-bandgap polymers is a promising strategy to achieve tandem solar cells with a very broad absorption range and high short circuit current.

Introduction

Solution processable thin-film photovoltaics show great potential in the search for cheap renewable energy sources. Rapid progress in recent years has seen single junction polymer-fullerene solar cells reach the 9 % efficiency mark.[1] However, the limitations of single junction solar cells have been extensively documented,[2–4] and interest is increasingly being shown in double or triple-junction solar cells.[5,6] By using materials with different bandgaps in a tandem structure, a broader coverage of the solar spectrum and, consequently, higher efficiency can be achieved. Recently, progress in the synthesis of efficient small-bandgap polymers has led to an increase of the efficiency of polymer tandem cells towards 9 % and absorption coverage extending to ~ 950 nm.[7,8] However, this accounts for only 71 % of the power available in the solar spectrum. Extension of the absorption spectrum further into the infrared is desirable, but highly efficient organic materials able to absorb further into the infrared are as yet lacking. Organically capped inorganic nanocrystals (also known as colloidal quantum dots) are a promising new class of solution processable semiconductors. For semiconducting nanocrystals with size smaller than the Bohr-radius of the exciton, spatial quantum confinement of the charge carriers leads to discretization of the energy levels and widening of the bandgap with respect to the bulk-value. Varying the QD size thus allows tuning of the bandgap and, correspondingly, of the absorption onset up to and even beyond that of Si.[9,10] At the same time, capping ligands provide solubility in organic solvents, thus opening the possibility of low-cost, low energy fabrication from solution. In this respect, colloidal quantum dots constitute a promising class of materials combining the beneficial properties of inorganic semiconductors, i.e. small-bandgaps and good transport properties, with the processability and versatility of organic semiconductors. In this work, we explore the use of PbS QDs in tandem solar cells to open the pathway to solution processable tandem solar cells with broad spectral coverage potentially beyond 1.1 μm.

PbS QDs have been used successfully in various device structures such as dye-sensitized solar cells,[11,12] Schottky type solar cells,[13–15] and depleted heterojunction solar cells where efficiencies of 7.3 % have been reported.[16–18] These successes notwithstanding, QDs have yet to be extensively explored in a tandem configuration. Serial tandem solar cells employing PbS QDs of different sizes for both the front and rear subcell have been reported by two research groups.[19,20] However, due to the high absorption coefficients in the visible spectral range regardless of the size of the PbS QDs, true absorption complementarity cannot be reached using nanocrystals only. To achieve a more uniform absorption coverage, PbS QDs can be used in combination with a suitably chosen polymer featuring a

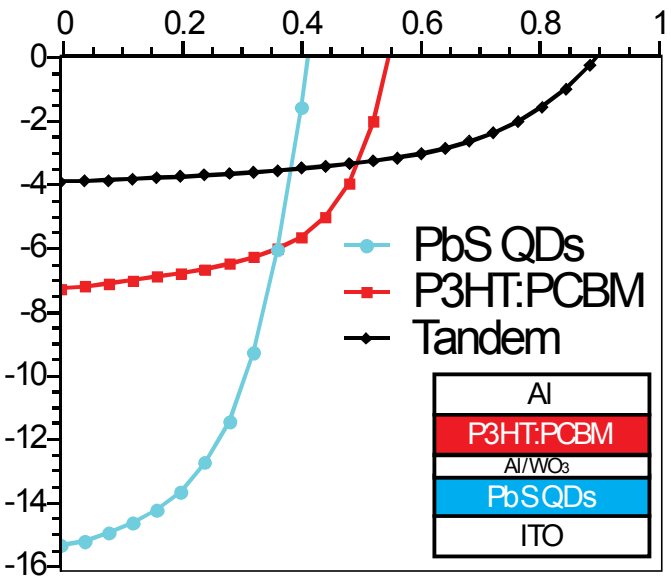

Fig. 1. J-V curves of the PbS single cell device (blue circles), the P3HT:PCBM single cell device (red squares), and the tandem device (black diamonds). The device structure of the tandem solar cell is displayed in the inset.

narrower absorption band, ideally with an onset around 900 nm. In this way, light would be harvested throughout the visible and into the infrared up to 1.1 µm. The combination of a QD and a polymer-fullerene subcell is therefore a promising, yet largely unexplored, strategy in achieving efficient tandem solar cells with broad spectral coverage.

Here we present the fabrication of a serial tandem solar cell employing PbS QDs as the front subcell and a blend of poly(3-hexylthiophene) (P3HT) and [6,6]-phenyl-C61-butyric acid methyl ester (PCBM) as the back subcell. The two cells are connected with an interlayer consisting of WO_3 and a thin layer of Al. These devices feature an open circuit voltage (V_{OC}) of 0.89 V, a short circuit current (J_{SC}) of 3.9 mA cm^{-2}, a fill factor (FF) of 53 %, and a power conversion efficiency (PCE) of 1.8 %. Finally, we present optical simulations which enlighten the potential of PbS QDs in various other tandem configurations.

Results and Discussion

The current-voltage (J-V) characteristics of the tandem cell and the reference cells can be seen in Fig. 1. The reference for the front subcell is an ITO/PbS/Al Schottky device, yielding a V_{OC} of 0.41 V, J_{SC} of 15.3 mA cm^{-2}, FF of 51 %, and a PCE of 3.0 %. The PbS film used for the reference was chosen to be slightly thicker than used in the tandem device to reduce the

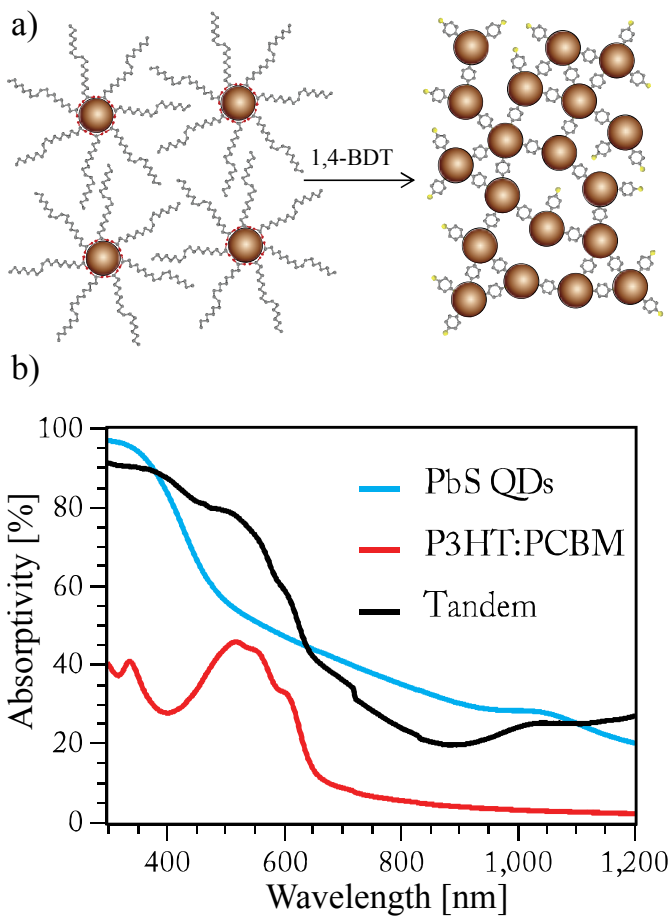

Fig. 2. a) Schematic representation of PbS QDs before and after replacement of the oleic acid ligands with 1,4-benzenedithiol. b) Absorption spectrum of the PbS QD reference cell (blue), the P3HT:PCBM single cell (red), and the tandem solar cell (black)

variance of the V_{OC}, as will be described later, giving rise to a slight overestimation of the V_{OC} of the reference cell and, consequently, a conservative estimation of the effectiveness of the interlayer. As a reference for the rear subcell, a P3HT:PCBM active layer is spincasted on top of ITO and WO_3, exhibiting a V_{OC} of 0.56 V, J_{SC} of 7.5 mA cm^{-2}, FF of 66 %, and a PCE of 2.7 %. The tandem configuration yielded a V_{OC} of 0.85 V, J_{SC} of 2.0 mA cm^{-2}, fill factor of 58 %, and a PCE of 1.0 %. The device characteristics are summarized in Table 1 and the EQE spectra of the subcells is shown in Figure S1. These results show that the WO_3 and Al together form an efficient interlayer for the recombination of the electrons from the bottom cell and the holes from the top cell, aligning the quasi-Fermi levels of the Al and WO_3 and resulting in a V_{OC} of the tandem cell equal to about 89 % of the sum of the respective subcells.

From the J_{SC}'s of the reference cells in Fig. 1, the P3HT:PCBM

Table 1. Device performance for tandem solar cells and respective reference devices.

Device Structure	PbS thickness [nm]	P3HT:PCBM thickness [nm]	V_{OC} [V]	J_{SC} [mA cm^{-2}]	FF [%]	PCE [%]
ITO/PbS/Al	110	-	0.41	15.2 ± 0.80	51	3.0 ± 0.16
ITO/WO_3/P3HT:PCBM/LiF/Al	-	105	0.56	7.5 ± 0.40	66	2.7 ± 0.14
ITO/PbS/Al/WO_3/P3HT:PCBM/LiF/Al	90	105	0.85	2.0 ± 0.20	58	1.0 ± 0.10

single cell provides about half the current of the PbS single cell. In the tandem structure, this discrepancy is exacerbated by the fact that the P3HT:PCBM is placed behind the PbS, which absorbs a large portion of the light in the visible, as can be seen in Fig. 2b. This results in a very low current generation in the rear cell and consequently a low J_{SC} in the tandem device. In addition, the slight loss in V_{OC} compared to the sum of the V_{OC}'s of the subcells may also be due to the large current mismatch. The excess of electrons supplied by the PbS subcell to the interlayer results in a negative space charge at the cathode of the front subcell. This space charge supplements the applied bias across the front cell and leads to a reduced contribution to the V_{OC} from that subcell. Therefore, we expect that both the J_{SC} and the V_{OC} of the tandem can be improved by better current matching.

To elucidate the mismatch in this device, optical modelling was performed to simulate the electromagnetic field as it propagates through the layers composing the device structure using the transfer matrix formalism.[21] This method requires as parameters only the wavelength-dependent complex refractive indices of all materials composing the device structure, and the thicknesses of each layer. In this model we assume that each absorbed photon contributes with one elementary charge to the current of the subcell, and that the current of the tandem is equal to the smallest of the currents produced by the two subcells. It should that be noted that in PbS QDs potentially more than one charge can be generated per photon through multiple exciton generation. However, without being able to quantify this effect, we choose to not make assumptions regarding the effect in our device. Where possible, values of the complex refractive indices were taken from literature,[22–25] and were otherwise obtained by variable angle spectral ellipsometry. The complex refractive indices of active layers used in this model can be found in Fig. S2.

Using this model, the current generated in both subcells as a function of the subcell thicknesses is simulated, yielding two current surfaces which can be seen in Fig. S3. If we take the minimum of the two surfaces we can obtain a simulated current of the tandem device as a function of the thicknesses of the subcells, displayed in Fig. 3 as a contour plot. The black line indicates at which thicknesses current matching is achieved between the subcells. Below the black line the current of the tandem device is limited by the PbS subcell, above the black line the tandem is limited by the P3HT:PCBM

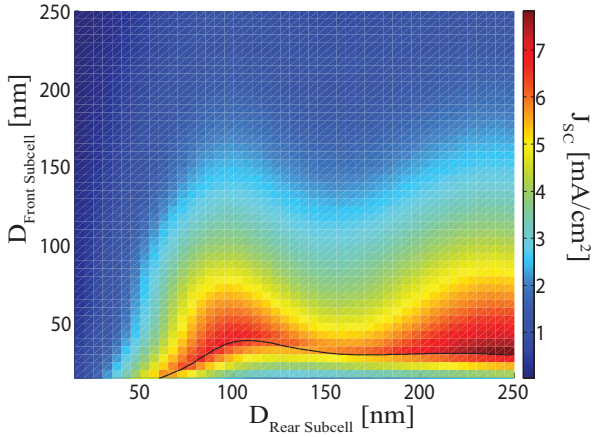

Fig. 3. Contour plot of the current of the tandem device assuming that each absorbed photon contributes one charge to the current of the subcells, and the current is equal to the smallest currents of the two subcells. The black line indicates the current matching condition between the subcells. Below the black line the current is limited by the PbS subcell, above the black line the tandem is limited by the P3HT:PCBM

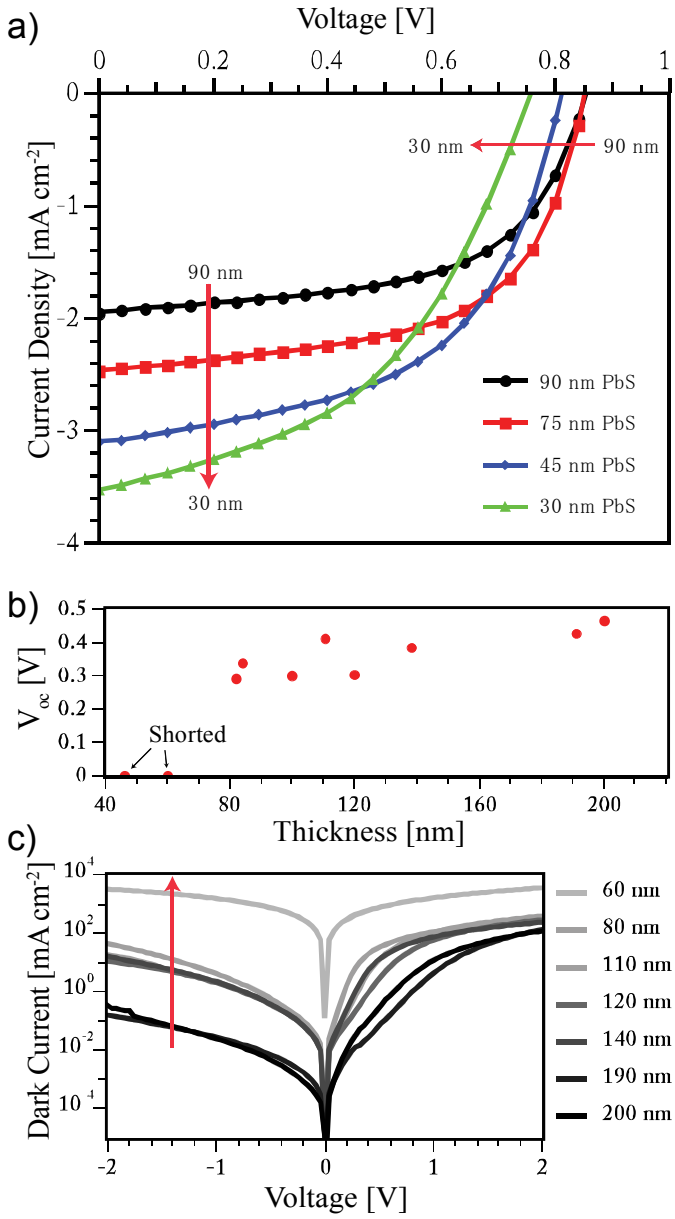

Fig. 4. a) J-V curves of the tandem structure for various PbS layer thicknesses. The J_{SC} increases as the thickness of the PbS subcell is reduced. The V_{OC} decreases due to decreased shunt resistance of the PbS subcell. b) The V_{OC} of ITO/PbS/LiF/Al Schottky devices for different PbS thickness. It can be seen that there is a large spread in the $V_{OC,}$ particularly for thin devices and a general trend to lower V_{OC} as the thickness is decreased. The J-V curves in the dark of these devices are displayed in c), showing increasing leakage in reverse bias as the thickness is decreased. This is symptomatic of low shunt resistance.

line the current is limited by the P3HT:PCBM subcell. The current matching condition cannot be achieved for PbS thicknesses exceeding ~ 40 nm. In addition, the current of the tandem device is strongly dependent on the thickness of the PbS layer and is only moderately sensitive to the P3HT:PCBM layer thickness. Therefore, the thickness of the PbS subcell was systematically tuned, and the experimental results are displayed in Fig. 4a. As expected, the J_{SC} was found to increase as the PbS thickness was decreased. Unexpectedly, however, decreasing the thickness also led to a decrease of the V_{OC} of the tandem device. We suggest that this is caused by decreasing shunt resistance in the PbS cell as the thickness is decreased, as can be seen in Fig. 4b-c. Low shunt resistance increases charge carrier recombination in the PbS layer and leads to a reduction of the V_{OC}. The decrease in shunt resistance is likely due to microscopic pinholes in the PbS film caused by the reduction of inter-nanocrystal spacing during the ligand exchange. While the QDs are capped with oleic acid, the inter-QD spacing is ~2 nm, which is reduced to ~0.5 nm when the ligand is replaced with the much shorter benzenedithiols.[26] This volume reduction causes pinholes or cracks of the topmost layer during fabrication. In thick devices, these pinholes are filled by the deposition of subsequent layers as the film is fabricated layer-by-layer. For thin devices, however, some pinholes may remain, leading to a low shunt resistance**.**

Therefore, in this case, decreasing the thickness of the front cell to the optically optimal value is not practically feasible. In a trade-off between J_{SC} and V_{OC}, an intermediate PbS thickness of ~ 60 nm and P3HT:PCBM thickness of 105 nm was chosen and optimized, resulting in a champion device featuring a V_{OC} of 0.89 V, J_{SC} of 3.9 mA cm^{-2}, FF of 53 % and a PCE of 1.8 %, the J-V characteristics are reported in Fig. 5. The open circuit voltage of this device is about 92 % of the sum of the subcell V_{OC}'s, which, to the best of our knowledge, is the best demonstration of WO_3 as a component for tandem device interlayers. WO_3 has been used previously in an interlayer in a serial tandem device by Janssen et al,[27] however in this work only 72 % of the sum of the subcell V_{OC}'s was obtained. To avoid the trade-off between better current matching and lower V_{OC}, the order of the subcells could be reversed, such that the lower absorbing P3HT subcell is in front and the PbS in the back. The optical modelling, displayed in Fig. S3 suggests that a J_{SC} of 9.5 mA cm^{-2} is theoretically possible in such a device. In addition, with the polymer in the front cell, high current can be achieved in a much broader range of thicknesses than with the polymer in the back. However, an even more promising approach would be to replace P3HT with a small band gap polymer as the front cell such as poly[2,6-(4,4-bis-(2-ethylhexyl)-4H-cyclopenta[2,1-b;3,4-b']-dithiophene)-alt-4,7-(2,1,3-benzothiadiazole)] (PCPDTBT),[28] and use PbS QDs as the rear cell. A maximum J_{SC} of 12.2 mA cm^{-2} is obtained from the modelling with this configuration. Further investigation of hybrid tandem devices combining PbS QDs with small band gap polymers is therefore promising.

Experimental Section

Nanocrystal synthesis: PbS QDs, capped with oleic acid ligands were synthesized using the hot injection method and treated with 4 washing steps. The full procedure is described elsewhere.[13] For this study, QDs featuring a first excitonic absorption peak at approximately 1025 nm in solution were used. The average diameter of the QDs was estimated to be around 3.4 nm using an empirical relationship between the first absorption peak and the particle size.[29]

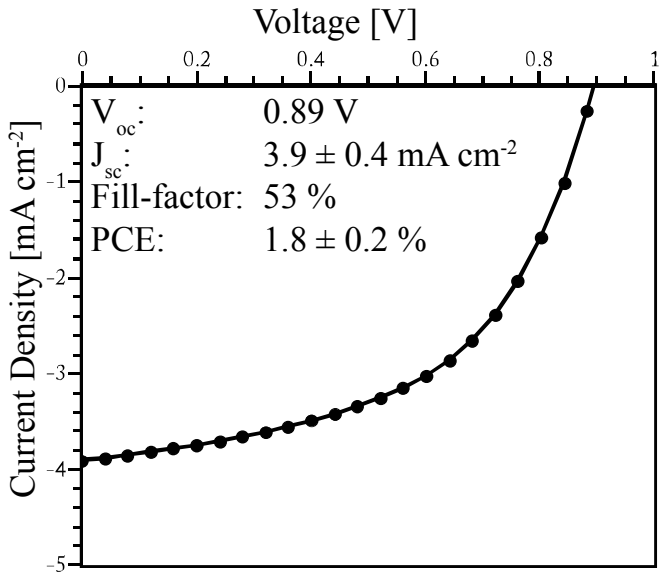

Fig. 5. J-V curve of the optimized tandem solar cell with 60 nm PbS front cell and 105 nm P3HT:PCBM rear cell.

Device fabrication: The device structure of the tandem cells is shown in the inset of Fig. 1. The layer of PbS was deposited onto a substrate of pre-patterned indium tin oxide (ITO) by a sequential layer-by-layer method whereby PbS is spincoated from chloroform, is subsequently treated with 1,4-benzenedithiol, and the procedure is repeated until the desired thickness is achieved. This treatment results in the replacement of the oleic acid ligands and in the crosslinking of the QDs into a dense, insoluble network, see Fig. 2a. As has been previously reported by our group,[13,14] the full removal of the oleic acid molecules in this manner is supported by FTIR spectra, as evidenced by the disappearance of the strong symmetrical and asymmetrical (COO-) vibrations at ~1400 and ~1550 cm^{-1} and the C-H vibrations at ~2856 and ~2925 cm^{-1}, which are typical of oleic acid. The interlayer was deposited by thermal evaporation of Al (1 nm), and WO_3 (15 nm). The rear active layer was spincoated from a solution of P3HT and PCBM (1:0.8 wt/wt) in 1,2-dichlorobenzene. The as-cast film was subsequently annealed at 120 °C for 5 minutes. The device was finished by thermal evaporation of LiF (1 nm) and Al (100 nm).

Measurements: Electrical characterization of the device was performed under simulated AM1.5G solar illumination using a Steuernagel SolarConstant 1200 lamp set to 100 mW cm^{-2} intensity using a silicon reference cell and corrected for the

spectral mismatch factor according to Kroon et al.[30] Ellipsometric data were obtained using a Woolham VASE ellipsometer, the data were fitted using Wvase32 software to obtain the complex refractive indices of the materials investigated.

Conclusions

In conclusion, tandem solar cells featuring PbS QDs as the front subcell and P3HT:PCBM as the rear subcell were fabricated, demonstrating the first hybrid inorganic-organic tandem solar cell where both subcells are processed from solution. An interlayer consisting of Al (1 nm) and WO_3 (15 nm) was implemented as an effective recombination layer, yielding a V_{OC} equal to about 92 % of the sum of the subcell V_{OC}'s. Optical modelling evidences that by replacing P3HT with a narrow bandgap polymer a substantial increase in the J_{SC} of the device can be obtained. Our approach provides a promising route to efficient solution processable tandem solar cells with spectral coverage up to 1.1 μm wavelength.

Acknowledgements

M. J Speirs and M. A. Loi acknowledge the financial support of the Alumnikring Den Haag/Rotterdam through the Ubbo Emmius Fund of the University of Groningen. M.A.L acknowledges also the support of the ERC Starting Grant "Hybrids Solution Processable Optoelectronic Devices" (Hy-SPOD) (ERC-306983).

[a] Zernike Institute for Advanced Materials, University of Groningen, Nijenborgh 4, Groningen, 9747 AG, The Netherlands
E-mail: m.j.speirs@rug.nl; m.a.loi@rug.nl.
[b] Department of Chemistry and Applied Biosciences, ETH Zürich, Wolfgang-Pauli-Str. 10, Zürich, 8093, Switzerland;
[c] EMPA-Swiss Federal Laboratories for Materials Science and Technology, Überlandstrasse 129, Dübendorf, 8600, Switzerland
E-mail: mvkovalenko@ethz.ch.

Electronic Supplementary Information (ESI) available: [Complex refractive indices of active layers; simulated current densities of the subcells and maximum theoretical J_{SC}'s of various tandem device architectures]. See DOI: 10.1039/c000000x/

1 Z. He, C. Zhong, S. Su, M. Xu, H. Wu, and Y. Cao, *Nat. Photonics*, 2012, **6**, 593.
2 W. Shockley and H. J. Queisser, *J. Appl. Phys*, 1961, **32**, 510.
3 M. Scharber and N. Sariciftci, *Prog. Polym. Sci.*, 2013, **38**, 1929.
4 G. Dennler, M. C. Scharber, T. Ameri, P. Denk, K. Forberich, C. Waldauf and C. J. Brabec, *Adv. Mat.*, 2008, **20**, 579.
5 T. Ameri, N. Li and C. J. Brabec, *Energy Environ. Sci.*, 2013, **6**, 2390.
6 T. Ameri, G. Dennler, C. Lungenschmied and C. J. Brabec, *Energy Environ. Sci.*, 2009, **2**, 347.
7 A. bin Mohd Yusoff, S. J. Lee, H. P. Kim, F. K. Shneider, W. J. da Silva and J. Jang, *Adv. Funct. Mater.*, 2013, doi: 10.1002/adfm.201303471.
8 W. Li, A. Furlan, K. H. Hendriks, M. M. Wienk and R. A. J. Janssen, *J. Am. Chem. Soc.*, 2013, **135**, 5529.
9 T. Rauch, M. Böberl, S. F. Tedde, J. Fürst, M. V. Kovalenko, G. Hesser, U. Lemmer, W. Heiss and O. Hayden, *Nat. Photonics*, 2009, **3**, 332.
10 K. Szendrei, F. Cordella, M. V. Kovalenko, M. Böberl, G. Hesser, M. Yarema, D. Jarzab, O. V. Mikhnenko, A. Gocalinska, M. Saba, F. Quochi, A. Mura, G. Bongiovanni, P. W. M. Blom, W. Heiss and M. A. Loi, *Adv. Mat.*, 2009, **21**, 683.
11 H. Lee, H. C. Leventis, S.-J. Moon, P. Chen, S. Ito, S. A. Haque, T. Torres, F. Nüesch, T. Geiger, S. M. Zakeeruddin, M. Grätzel and M. K. Nazeeruddin, *Adv. Funct. Mater.*, 2009, **19**, 2735.
12 R. Plass, S. Pelet, J. Krueger, M. Grätzel and U. Bach, *J. Phys. Chem. B*, 2002, **106**, 7578.
13 C. Piliego, L. Protesescu, S. Z. Bisri, M. V. Kovalenko and M. A. Loi, *Energy Environ. Sci.*, 2013, **6**, 3054.
14 K. Szendrei, W. Gomulya, M. Yarema, W. Heiss and M. Loi, *Appl. Phys. Lett.*, 2010, **97**, 203501.
15 J. Tang, X. Wang, L. Brzozowski, D. A. R. Barkhouse, R. Debnath, L. Levina and E. H. Sargent, *Adv. Mat.*, 2010, **22**, 1398.
16 H. Wang, T. Kubo, J. Nakazaki, T. Kinoshita and H. Segawa, *J. Phys. Chem. Lett.*, 2013, **4**, 2455.
17 X. Lan, J. Bai, S. Masala, S. M. Thon, Y. Ren, I. J. Kramer, S. Hoogland, A. Simchi, G. I. Koleilat, D. Paz-Soldan, Z. Ning, A. J. Labelle, J. Y. Kim, G. Jabbour and E. H. Sargent, *Adv. Mat.*, 2013, **25**, 1768.
18 A. G. Pattantyus-Abraham, I. J. Kramer, A. R. Barkhouse, X. Wang, G. Konstantatos, R. Debnath, L. Levina, I. Raabe, M. K. Nazeeruddin, M. Grätzel and E. H. Sargent, *ACS Nano*, 2010, **4**, 3374.
19 X. Wang, G. I. Koleilat, J. Tang, H. Liu, I. J. Kramer, R. Debnath, L. Brzozowski, D. A. R. Barkhouse, L. Levina, S. Hoogland and E. H. Sargent, *Nat. Photonics*, 2011, **5**, 480.
20 J. J. Choi, W. N. Wenger, R. S. Hoffman, Y. F. Lim, J. Luria, J. Jasieniak, J. A. Marohn and T. Hanrath, *Adv. Mat.*, 2011, **23**, 3144.
21 L. A. A. Pettersson, L. S. Roman and O. Inganäs, *J. Appl. Phys.*, 1999, **86**, 487.
22 A. D. Rakić, *Appl. Opt.*, 1995, **34**, 4755.
23 H. Hoppe, S. Shokhovets and G. Gobsch, *Phys. Status Solidi*, *RRL* 2007, **1**, R40.
24 T. Ameri, G. Dennler, C. Waldauf, H. Azimi, A. Seemann, K. Forberich, J. Hauch, M. Scharber, K. Hingerl and C. J. Brabec, *Adv. Funct. Mater.*, 2010, **20**, 1592.
25 J. D. Kotlarski, P. W. M. Blom, L. Koster, M. Lenes and L. H. Slooff, *J. Appl. Phys.*, 2008, **103**, 084502.
26 K. Szendrei, M. J. Speirs, W. Gomulya, D. Jarzab, M. Manca, O. V. Mikhnenko, M. Yarema, B. J. Kooi, W. Heiss and M. A. Loi, *Adv. Funct. Mater.*, 2012, **22**, 1598.
27 A. Janssen, T. Riedl, S. Hamwi, H. H. Johannes and W. Kowalsky, *Appl. Phys. Lett.*, 2007, **91**, 073519.
28 J. Peet, J. Kim, N. E. Coates, W. L. Ma, D. Moses, A. J. Heeger and G. C. Bazan, *Nat. Materials*, 2007, **6**, 497.
29 I. Moreels, K. Lambert, D. Smeets, D. De Muynck, T. Nollet, J. Martins, F. Vanhaecke, A. Vantomme, C. Delerue, G. Allan and Z. Hens, *ACS Nano*, 2009, **3**, 3023.

30 J. Kroon, M. Wienk, W. Verhees and J. Hummelen, *Thin Solid Films*, 2002, **403**, 223.

